Statistical Characterization of Time-Dependent Variability Defects Using the Maximum Current Fluctuation

P. Saraza-Canflanca, J. Martin-Martinez, R. Castro-Lopez, E. Roca, R. Rodriguez, *Member, IEEE*, F. V. Fernandez, *Member, IEEE,* and M. Nafria, *Senior Member, IEEE*

***Abstract*— This article presents a new methodology to extract, at a given operation condition, the statistical distribution of the number of active defects that contribute to the observed device time-dependent variability, as well as their amplitude distribution. Unlike traditional approaches based on complex and time-consuming individual analysis of thousands of current traces, the proposed approach uses a simpler trace processing, since only the maximum and minimum values of the drain current during a given time interval are needed. Moreover, this extraction method can also estimate defects causing small current shifts, which can be very complex to identify by traditional means. Experimental data in a wide range of gate voltages, from near-threshold up to nominal operation conditions, are analyzed with the proposed methodology.**

***Index Terms*— Bias temperature instability (BTI), maximum current fluctuation (MCF), random telegraph noise (RTN), time-dependent variability (TDV), transistor.**

I. Introduction

TIME-DEPENDENT variability (TDV), caused by phenomena such as random telegraph noise (RTN) and bias temperature instability (BTI), has become a subject of increasing concern in deeply scaled CMOS technologies [1], due to its role as a source of device and circuit performance variability [2], [3]. At device level, RTN is observed as discrete jumps of the drain current. It is generally accepted that these current shifts are caused by the stochastic trapping/detrapping of charge carriers in/from defects. In particular, when charge carriers are trapped in defects, they change the density of charge located at the silicon–oxide interface, which causes an increase in the threshold voltage of the device, thus decreasing its drain current [4], [5]. Detrapping of carriers from defects has, therefore, the opposite impact on the device current. Because of the stochastic nature of the phenomenon, the threshold voltage shifts (or, equivalently, current jumps) are statistically distributed. BTI is also associated with the same kind of phenomena; though, in this case, charge detrapping is mainly observed when gate bias is decreased (a phase known as recovery). However, some of the carriers may not be detrapped, leading to a permanent shift of the threshold voltage, consequently degrading the device performance [6]. In ultrascaled devices, the recovery phase is observed as sudden increments in the drain current, similar to RTN current shifts. In fact, there is a general consensus that RTN and the recoverable component of BTI are caused by the same type of defects [4], [7], and the observation of one phenomenon or the other actually depends on the operation conditions (voltage, time, temperature).

Then, nowadays both phenomena are usually described in the context of defect-centric models [7]–[10], which account for the variations in the transistor threshold voltage caused by the trapping/detrapping of charge carriers in/from defects present in the devices. To assess the impact on circuit performances, it is crucial to characterize these phenomena and extract the statistical distributions of the main parameters that describe them.

The characterization of RTN and BTI defects traditionally relies on the detailed analysis of individual current traces [11]–[13]. This analysis detects the number of transitions with a distinct amplitude, each one of them corresponding to a different defect, or the total number of current levels. From any of these values, the number of defects can be easily calculated. However, these conventional approaches are convoluted and error-prone to the point that they are unable to correctly extract the number of defects and their associated current shifts when: 1) the trace is very complex (i.e., with a large number of distinct transitions, particularly if some of these transitions have similar associated current amplitudes); 2) some of the defects produce current shifts with an amplitude below the noise level; or 3) the defect characteristics are around the measurement equipment resolution. In this article, we propose a method based on a new metric, the maximum

Manuscript received March 22, 2021; revised May 10, 2021 and May 21, 2021; accepted May 31, 2021. Date of publication June 17, 2021; date of current version July 23, 2021. This work was supported in part by the VIGILANT Project under Grant PID2019-103869RB/AEI/10.13039/501100011033 and in part by the TEC2016-75151-C3-R Project under Grant AEI/FEDER, UE. The work of P. Saraza-Canflanca was supported by the Ministry of Science and Innovation (MICINN) under Grant BES-2017-080160. The review of this article was arranged by Editor E. A. Gutiérrez-D. *(Corresponding author: J. Martin-Martinez.)*

P. Saraza-Canflanca, R. Castro-Lopez, E. Roca, and F. V. Fernandez are with the Instituto de Microelectrónica de Sevilla, (Universidad de Sevilla, CSIC), 41012 Seville, Spain (e-mail: francisco.fernandez@imse-cnm.csic.es).

J. Martin-Martinez, R. Rodriguez, and M. Nafria are with the Department of Electronic Engineering, Universitat Autònoma de Barcelona, 08193 Bellaterra, Spain (e-mail: javier.martin.martinez@uab.cat).

Color versions of one or more figures in this article are available at https://doi.org/10.1109/TED.2021.3086448.

Digital Object Identifier 10.1109/TED.2021.3086448

current fluctuation (MCF), to obtain the distribution of the number of active TDV-related defects (i.e., defects that suffer at least one trapping/detrapping event) and their associated current shifts, δI, that: 1) accounts for all active defects and 2) does not require any complex analysis of the experimental current traces, since only a very rough estimation of the current shift distribution (easier to obtain) and the upper and lower bounds of the current are required. This model describes the experimental data accurately at gate voltages ranging from the near-threshold region to the nominal operation voltage of the technology.

The rest of this article is structured as follows. First, in Section II, the MCF methodology used in this work is explained. Then, in Section III, the results obtained using this methodology are presented. Finally, in Section IV, conclusions are drawn.

II. Methodology Description

In the following, a metric is introduced to easily extract the defect-centric model parameters, i.e., the number of active defects and their associated current jumps, from experimental current traces.

Consider the current trace shown in Fig. 1(a) corresponding to a PMOS device of $W/L = 80$ nm/60 nm biased with $|V_{GS}| = 1.2$ V and $|V_{DS}| = 0.1$ V. We define the cumulative maximum current (CMAXC) at any time instant t' within the experimental window as the maximum current within the interval $0 \leq t \leq t'$

$$\text{CMAXC}(t') = \max_{\forall t \in [0,t']} I(t). \tag{1}$$

CMAXC is plotted in Fig. 1(a) with the orange line. Similarly, the cumulative minimum current (CMINC) at any time instant t' within the experimental window is defined as

$$\text{CMINC}(t') = \min_{\forall t \in [0,t']} I(t) \tag{2}$$

and is plotted in Fig. 1(a) with a lower blue line. Finally, the metric proposed in this article, the MCF, is defined as the difference between both

$$\text{MCF}(t') = \text{CMAXC}(t') - \text{CMINC}(t'). \tag{3}$$

Notice that, although current transitions caused by TDV defects are bipolar (i.e., charge trapping/detrapping events decrease/increase the drain current), the MCF metric is, according to its definition, unipolar (i.e., the difference between the maximum and minimum values of the current will always be a positive value and MCF(t) an ever-increasing function).

Due to the TDV stochasticity, each device shows a different MCF trace. In fact, the MCF value for a given device at a time t can be expressed as

$$\text{MCF}(t) = \sum_{i=1}^{N} \delta I_i + \varepsilon_{\text{noise}} \tag{4}$$

where N represents the number of active defects (i.e., defects that have captured/emitted a charge carrier at least once) from the beginning of the time window up to time t, and δI_i represents the current shift associated with the trapping/detrapping in/from each of those defects. The term $\varepsilon_{\text{noise}}$ accounts for the contribution of the background noise to the MCF.

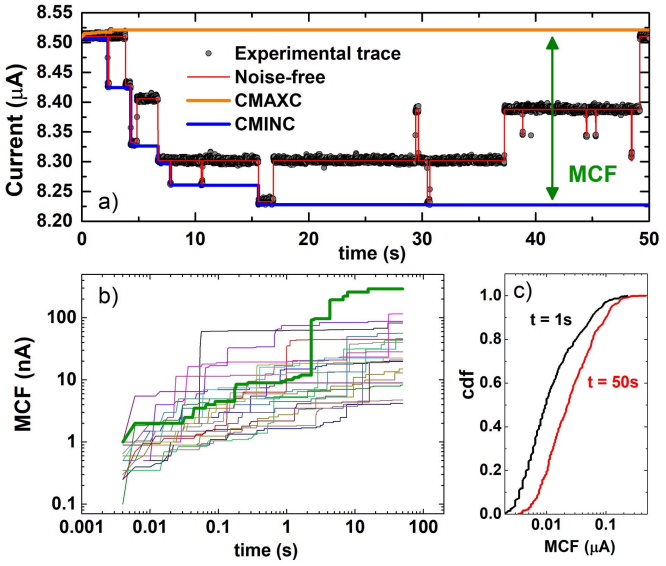

Fig. 1. (a) Experimental current trace and current bounds from which the MCF is computed. The arrow indicates the MCF at around $t = 41$ s. (b) MCF(t) obtained from 20 current traces (the one in (a) is highlighted in green). (c) cdf of the MCFs for $t = 1$ s and $t = 50$ s for a set of 500 transistors.

Fig. 1(b) shows the temporal evolution of the MCFs of 20 CMOS transistors. From these data, the cumulative distribution function (cdf) of the MCF can be obtained for a particular time instant, as shown in Fig. 1(c). Notice in Fig. 1(c) that the distribution of the MCF values shift to larger values when longer times are considered. This is expected, since a larger number of active defects may be present in longer measurement windows (e.g., 50 s) than in shorter ones (e.g., 1 s). In fact, the MCF for a single device depends on the number of active defects, N, and their current shifts, δI, associated with their occupancy state, as shown in (4). Therefore, at each time t, there is a unique distribution of N that, together with the δI distribution, correctly describes the experimental MCF distribution. The extraction of both distributions is the goal of this work.

Note that the parameters (N and δI) that are needed by the MCF-based methodology to describe and predict the impact of TDV defects on the transistor characteristics can be easily related to those of defect-centric TDV models, such as the probabilistic defect occupancy (PDO) model [9]. The necessary parameters to construct such model are the total number of defects in the device (N_T), the distribution of the capture and emission time constants of the defects (τ_c, τ_e), which determine for each defect its probability of being occupied or empty, and the distribution of the amplitudes of the shifts associated with each defect when occupied, δI. These variables can be easily related to those used in this work. First, the number of active defects N extracted through the MCF-based methodology depends on the total number of defects in the device, N_T, and on the time constants (τ_c, τ_e).

For each defect, its time constants determine if the device will be active (i.e., suffer at least one trapping/detrapping event) during a given time window, in particular, during the time interval between the start of the measurement and the time instant in which the cdf of the MCF is calculated (e.g., a defect with $\tau_c \approx \tau_e \approx 1$ s will surely be accounted as an active defect during a measurement yielding the calculation of MCF at 50 s). Finally, the distribution of the amplitudes of the shifts considered in defect-centric models is equivalent to the δI distribution considered in this work.

A related but different metric, the within device fluctuation (WDF), has been presented in [14] and [15]. However, though somehow related, they should not be confused, since they have been defined with different goals. The WDF metric for a time instant t' is given by the difference between $\mathrm{Max}(t')$ and $\mathrm{Min}(t')$. $\mathrm{Max}(t')$ is given by the maximum current increase from the start of the measurement up to t' (hence, it is directly related to our definition of CMAXC), and $\mathrm{Min}(t')$ is given by the minimum current variation from the end of the measurement window down to t' [14] (thus different from CMINC). A major difference between both metrics is that the WDF value at intermediate time instants depends on the size of the measurement time window, e.g., the value of $\mathrm{Min}(t')$ for the trace in Fig. 1(a) for time instants between 18 and 30 s is different if the measurement window extends to 30 or 50 s. This brings along an important consequence: the value of the WDF metric is only reliable for time instants sufficiently below the measurement window [14]. In any case, the WDF metric is, in itself, not appropriate for our purposes in this article, since the $\mathrm{Min}(t')$ values at intermediate time instants would be determined by the current variation at the later time instants. Hence, it cannot be related to the number of active defects and their associated current jumps at those intermediate time instants, which is the goal of this article.

To expose the limitations of time-consuming conventional approaches, an attempt has been made to extract the amplitudes of the current shifts caused by the trapping/detrapping events of individual defects from experimental data. In order to get statistically relevant data, RTN traces have been measured in 500 PMOS transistors of $W/L = 80$ nm/60 nm (integrated into an IC fabricated in a commercial 65-nm planar CMOS technology specifically designed for TDV characterization) with $|V_{DS}| = 0.1$ V and different gate voltages, $|V_{GS}| = 0.6$, 0.7, 0.8, 1.0, and 1.2 V, for 50 s. Details about the IC and the measurement setup can be found in [16] and [17]. Fig. 1(a) shows an example of noise-free RTN trace (red trace), obtained using the method in [11]. Noise-free trace here refers to the result of a mathematical processing that eliminates small current shifts due to background noise including, e.g., thermal noise of the devices or noise of the measurement equipment, hence, obtaining a clean trace that clearly shows the effect of RTN. From the noise-free RTN traces, δI caused by each defect is extracted. Using this procedure, hundreds of δI values were determined for each bias condition. Fig. 2(a) depicts the experimental cdfs obtained for the δI distributions for the different biasing voltages, which can be correctly fitted considering two lognormal distributions. Fig. 2(b) displays

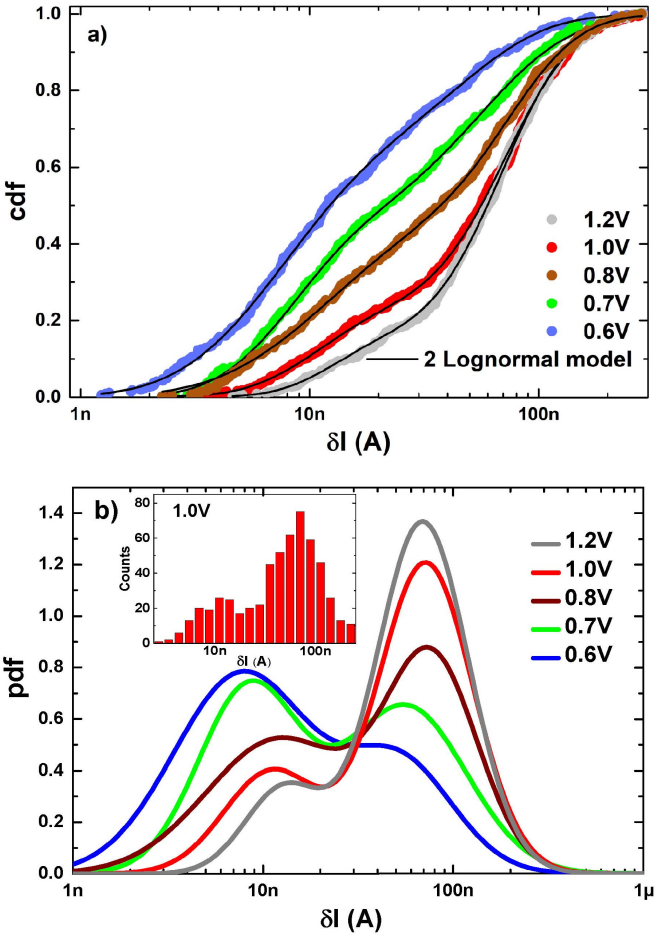

Fig. 2. (a) δI cdf and fitted two-lognormal model (black lines). (b) Corresponding pdfs of the fitted two-lognormal model. The inset in (b) displays the histogram for the experimentally extracted amplitudes for one of the bias conditions ($|V_{GS}| = 1$ V).

the corresponding probability density functions (pdfs) of the fitted two-lognormal model. The inset in Fig. 2(b) shows the experimental histogram constructed with the values of δI extracted at one of the bias conditions, which reinforces the suitability of a two-lognormal model. The two lognormal functions in the RTN amplitude distribution could originate from two categories of traps, located above the percolation path or not, which cause larger or smaller RTN amplitudes, respectively [18]. In any case, notice that no assumption has been done for the selection of this type of distribution, but rather has been found to properly fit the experimental data. In fact, only by using high-resolution equipment, which allows the measurement of current jumps in the nanoampere range, the lognormal corresponding to the smaller amplitudes shows up.

Using these distributions and assuming a Poisson distribution with mean value $\langle N \rangle$ for the number of defects [19], the experimental MCF distributions can be fitted. An example is shown in Fig. 3 (blue line) for $|V_{GS}| = 1.2$ V and $t = 100$ ms, which has made use of the 1.2-V δI distribution in Fig. 2. Clearly, the larger values (above 50 nA) of the MCF distribution can be properly described using this approach. However, it fails to describe the smaller MCF

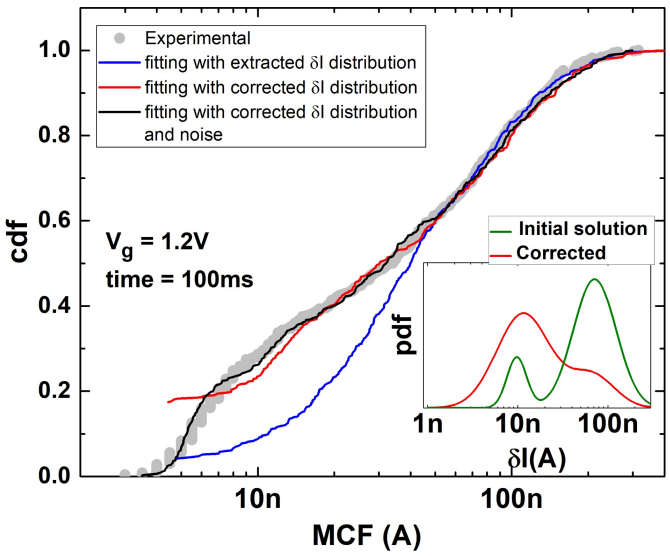

Fig. 3. MCF experimental distribution (gray symbols) and fitting (lines) considering the extracted and corrected δI distributions. The inset shows (green) the initial guess of the δI distribution considered for the MCF distribution fitting and (red) δI distribution that better fits the distribution.

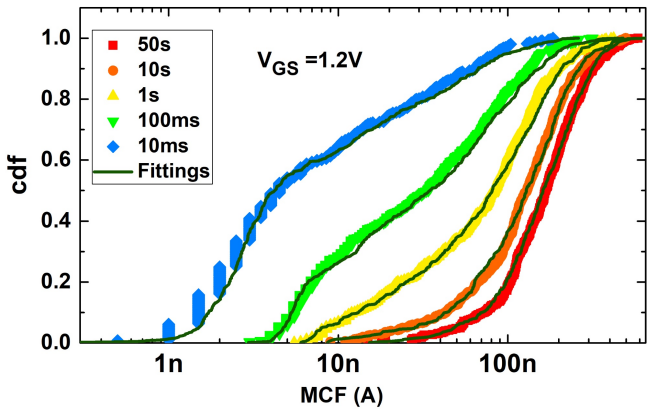

Fig. 4. Experimental MCF distributions obtained at different times (symbols) and fittings using the proposed technique (solid lines).

values, because the δI distribution is obtained from the experimental current traces [as that in Fig. 1(a)], where, as mentioned in Section I, a portion of defects, especially those with small δI, have not been detected (due to experimental limitations) and yet these affect the MCF calculation, and are, therefore, accounted for by the MCF-based methodology. In fact, low-δI detection problem is a common issue of any method extracting δI, and consequently N, from experimental RTN traces [11], [19], [20], which are not able to detect defects that have an associated low-amplitude current shift. This reinforces the idea that conventional processing techniques may not only require a complex and time-consuming analysis, but may also lead to an erroneous characterization of the distribution of the number of defects and their associated amplitudes.

To solve this inaccuracy, we postulate here that the MCF metric can be useful even without a detailed, time-consuming analysis of the traces to attain a δI distribution (as in Fig. 2). In fact, these painstakingly derived δI distributions are not really required. To illustrate this, the N distribution and a corrected δI distribution (red curve in the inset in Fig. 3) have been obtained by minimizing the difference between the MCF cdf in Fig. 3 (red curve) and the experimental one (gray dots). Notice that the δI distributions in Fig. 2 are not used for this MCF distributions fittings. Instead, for proper convergence of the fitting procedure, a very rough initial approximation (green curve in the inset in Fig. 3) is obtained from those traces (150 of 500) that contain one clear defect (only two current levels separated by at least 5 nA). This approximated δI distribution is faster and easier to extract and does not require a detailed, complex, and painstakingly processing of every shift, both large and small, in every current trace, as required to get the distributions in Fig. 2.

An additional fact must be considered when trying to fit the experimental cdf of the MCF in Fig. 3: so far, devices without defects lead to simulated MCF $= 0$, while, experimentally, MCF will be always higher than zero due to the background noise. To solve this discrepancy, a Gaussian background noise with standard deviation obtained from the experimental data is added to the generation of the MCF values. Then, the experimental MCF distribution can be more accurately fitted (black line in Fig. 3) in the whole range. In summary, the experimental MCF distribution can be correctly described by just considering a Poisson distribution of N with mean value $\langle N \rangle$ (1.8, for the case shown in Fig. 3), the corrected δI distribution (red line in inset of Fig. 3) originated from an easy-to-attain, rough δI distribution approximation, and a Gaussian background noise.

III. Results

Once the MCF-based methodology has been explained, the next step is to analyze the MCF time dependency. Fig. 4 shows the MCF distributions for different measurement intervals considering sections of the measured traces up to 10 ms, 100 ms, 1 s, 10 s, and 50 s. As expected, the MCF distributions shift to higher values for longer times. This is attributed to the fact that in longer current traces, more defects can be activated, and, therefore, higher MCF values are encountered from the traces. Interestingly enough, the experimental MCF distributions can be well reproduced with our approach by simply varying the mean value of the active defects, $\langle N \rangle$, without any modification of the previously corrected δI distribution or the background noise. This implies that there is no correlation between the current shift associated with a defect and its time constants [21].

The approach illustrated above for $|V_{GS}| = 1.2$ V has been applied to other operation conditions. Fig. 5(a) shows the evolution of $\langle N \rangle$ with time for all the applied values of V_{GS}, which can be described using a bias-dependent lognormal-type distribution. Fig. 5(b) shows the Poisson distribution for the number of defects for $t = 50$ s at different bias conditions.

Table I displays the main parameters extracted through the MCF-based procedure, namely, the distribution of the current shifts associated with the trapping/detrapping of defects, and the number of such active defects with respect to the

TABLE I
PARAMETERS EXTRACTED FOR THE δI DISTRIBUTION OF RTN DEFECTS AND THE TIME EVOLUTION OF $\langle N \rangle$

$\lvert V_{gs} \rvert$	K	μ_l	σ_l	μ_u	σ_u	N_0	μ_N	σ_N
0.6V	0.86	-7.95	0.07	-7.25	0.26	9.77	4.14	2.93
0.7V	0.77	-7.94	0.09	-7.16	0.22	9.87	3.21	2.51
0.8V	0.64	-8.05	0.13	-7.18	0.29	10.20	3.02	2.56
1V	0.76	-8.07	0.21	-7.15	0.25	9.85	1.59	2.14
1.2V	0.80	-7.91	0.12	-7.18	0.25	10.37	0.78	1.84

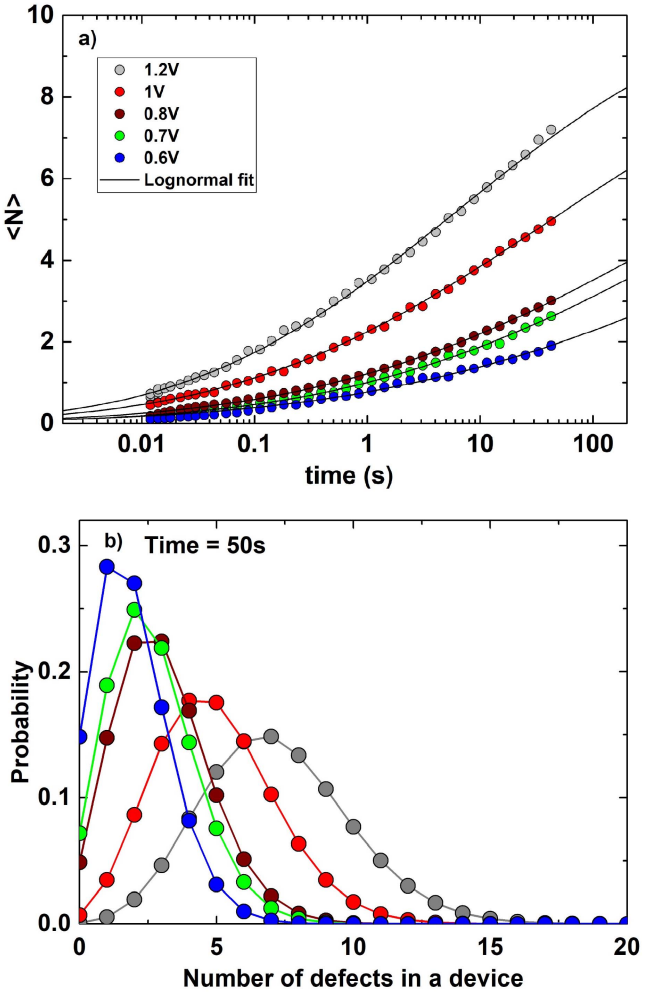

Fig. 5. (a) Time evolution of $\langle N \rangle$ (symbols), which can be described using a lognormal-type distribution (lines). (b) Poisson distributions at $t = 50$ s.

operation time. Specifically, the parameters correspond to fitting the following distribution for the current shifts:

$$\mathrm{cdf}(\delta I) = \frac{K}{2}\left[1 + \mathrm{erf}\left(\frac{\log(\delta I) - \mu_l}{\sigma_l\sqrt{2}}\right)\right] + \frac{(1-K)}{2}\left[1 + \mathrm{erf}\left(\frac{\log(\delta I) - \mu_u}{\sigma_u\sqrt{2}}\right)\right] \quad (5)$$

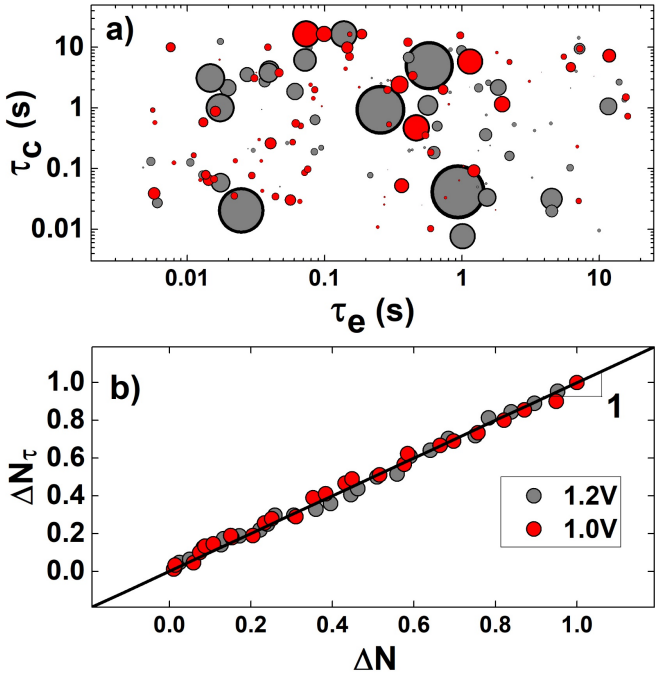

Fig. 6. (a) Experimental τ_e and τ_c values obtained from the analysis of individual RTN traces. The size of the symbols represents δI associated with each defect. (b) Portion of the total active defects at a given time interval, ΔN, extracted using the MCF-based method, versus the relative number of defects, ΔN_τ, obtained from the analysis of individual traces (a).

where erf() is the error function, μ_l and μ_u, σ_l and σ_u represent the mean and standard deviation of the lower and upper lognormal function, and K represents the relative amplitude of both distributions. And for the number of defects

$$\langle N \rangle(t) = \frac{N_0}{2}\left[1 + \mathrm{erf}\left(\frac{\log(t) - \mu_N}{\sigma_N\sqrt{2}}\right)\right]. \quad (6)$$

Using these parameters, it is possible to predict the impact of the current fluctuations on the overall device drain current, as when using other defect-centric models such as the PDO model [9].

Finally, to further illustrate the proposed methodology, the following test has been performed. From the detailed analysis of hundreds of individual RTN traces measured at $|V_{GS}| = 1$ and 1.2 V, many emission (τ_e)/capture (τ_c) times

have been extracted [Fig. 6(a)]. With these data, the number of defects N_τ that will be active within a given time window has been calculated, assuming that defects will be active within a given time window t if their corresponding τ_e and τ_c are smaller than t. When the relative variation of the number of defects, ΔN_τ, in a given time interval is plotted against the equivalent variation evaluated using the MCF-based method, ΔN, a linear relation between them for the voltages considered is observed [Fig. 6(b)]. This result indicates that the same temporal trend is obtained for the number of defects that will be active, whether predicted by the novel MCF-based technique presented in this article or extracted by performing a time-consuming, massive analysis of individual current traces. However, the procedure here presented is much simpler and more straightforward than the identification of individual defects from a large set of traces, while accounts for all the active defects in the device within the experimental time window, regardless of their amplitude.

IV. Conclusion

In deeply scaled CMOS technologies, TDV phenomena, such as RTN and BTI, display a stochastic nature, caused by the trapping/detrapping of charge carriers in/from individual defects. To account for this stochastic behavior, it is fundamental to develop accurate and automated methods to accurately characterize those phenomena.

This article presents a novel methodology using a new metric, MCF, to evaluate the distributions of the number of active TDV-related defects and their associated current shifts within a given time window and under given operation conditions. Unlike conventional methods that analyze current traces, this method relies on a rather uncomplicated processing. It has also been shown that the MCF-based methodology is able to obtain a more precise distribution of the defect current amplitudes than conventional techniques, often failing at detecting defects with low-amplitude current shifts.

References

[1] N. Tega *et al.*, "Increasing threshold voltage variation due to random telegraph noise in FETs as gate lengths scale to 20 nm," in *Proc. IEEE Symp. VLSI Technol.*, Jun. 2009, pp. 50–51.

[2] N. Tega *et al.*, "Impact of threshold voltage fluctuation due to random telegraph noise on scaled-down SRAM," in *Proc. IEEE Int. Rel. Phys. Symp.*, Apr. 2008, pp. 541–546, doi: 10.1109/RELPHY.2008.4558943.

[3] M. Luo, R. Wang, S. Guo, J. Wang, J. Zou, and R. Huang, "Impacts of random telegraph noise (RTN) on digital circuits," *IEEE Trans. Electron Devices*, vol. 62, no. 6, pp. 1725–1732, Jun. 2015, doi: 10.1109/TED.2014.2368191.

[4] T. Grasser *et al.*, "Switching oxide traps as the missing link between negative bias temperature instability and random telegraph noise," in *IEDM Tech. Dig.*, Dec. 2009, pp. 1–4, doi: 10.1109/IEDM.2009.5424235.

[5] T. Grasser, "Stochastic charge trapping in oxides: From random telegraph noise to bias temperature instabilities," *Microelectron. Rel.*, vol. 52, no. 1, pp. 39–70, Jan. 2012, doi: 10.1016/j.microrel.2011.09.002.

[6] T. Grasser *et al.*, "The 'permanent' component of NBTI: Composition and annealing," in *Proc. IEEE Int. Rel. Phys. Symp. (IRPS)*, 2011, pp. 6A.2.1–6A.2.9, doi: 10.1109/IRPS.2011.5784543.

[7] T. Grasser, K. Rott, H. Reisinger, M. Waltl, J. Franco, and B. Kaczer, "A unified perspective of RTN and BTI," in *Proc. IEEE Int. Reliability Phys. Symp. (IRPS)*, Jun. 2014, pp. 4A.5.1–4A.5.7, doi: 10.1109/IRPS.2014.6860643.

[8] B. Kaczer *et al.*, "The defect-centric perspective of device and circuit reliability—From individual defects to circuits," in *Proc. 45th Eur. Solid State Device Res. Conf. (ESSDERC)*, Sep. 2015, pp. 218–225, doi: 10.1109/ESSDERC.2015.7324754.

[9] J. Martin-Martinez *et al.*, "Probabilistic defect occupancy model for NBTI," in *Proc. Int. Rel. Phys. Symp.*, 2011, pp. XT.4.1–XT.4.6, doi: 10.1109/IRPS.2011.5784605.

[10] N. Ayala, J. Martin-Martinez, R. Rodriguez, M. Nafria, and X. Aymerich, "Unified characterization of RTN and BTI for circuit performance and variability simulation," in *Proc. Eur. Solid-State Device Res. Conf. (ESSDERC)*, Sep. 2012, pp. 266–269, doi: 10.1109/ESSDERC.2012.6343384.

[11] P. Saraza-Canflanca *et al.*, "A robust and automated methodology for the analysis of time-dependent variability at transistor level," *Integration*, vol. 72, pp. 13–20, May 2020, doi: 10.1016/j.vlsi.2020.02.002.

[12] T. Nagumo, K. Takeuchi, S. Yokogawa, K. Imai, and Y. Hayashi, "New analysis methods for comprehensive understanding of random telegraph noise," in *IEDM Tech. Dig.*, Dec. 2009, pp. 1–4, doi: 10.1109/IEDM.2009.5424230.

[13] J. Martin-Martinez, J. Diaz, R. Rodriguez, M. Nafria, and X. Aymerich, "New weighted time lag method for the analysis of random telegraph signals," *IEEE Electron Device Lett.*, vol. 35, no. 4, pp. 479–481, Apr. 2014, doi: 10.1109/LED.2014.2304673.

[14] M. Duan *et al.*, "New analysis method for time-dependent device-to-device variation accounting for within-device fluctuation," *IEEE Trans. Electron Devices*, vol. 60, no. 8, pp. 2505–2511, Aug. 2013.

[15] M. Duan *et al.*, "Time-dependent variation: A new defect-based prediction methodology," in *Symp. VLSI Technol. (VLSI-Technol.) Dig. Tech. Papers*, Jun. 2014, pp. 1–2, doi: 10.1109/VLSIT.2014.6894373.

[16] J. Diaz-Fortuny *et al.*, "A versatile CMOS transistor array IC for the statistical characterization of time-zero variability, RTN, BTI, and HCI," *IEEE J. Solid-State Circuits*, vol. 54, no. 2, pp. 476–488, Feb. 2019, doi: 10.1109/JSSC.2018.2881923.

[17] J. Diaz-Fortuny *et al.*, "Flexible setup for the measurement of CMOS time-dependent variability with array-based integrated circuits," *IEEE Trans. Instrum. Meas.*, vol. 69, no. 3, pp. 853–864, Mar. 2020, doi: 10.1109/TIM.2019.2906415.

[18] Z. Zhang *et al.*, "New insights into the amplitude of random telegraph noise in nanoscale MOS devices," in *Proc. IEEE Int. Rel. Phys. Symp. (IRPS)*, Apr. 2017, pp. 3C-3.1–3C-3.5, doi: 10.1109/IRPS.2017.7936288.

[19] P. Weckx, B. Kaczer, C. Chen, P. Raghavan, D. Linten, and A. Mocuta, "Relaxation of time-dependent NBTI variability and separation from RTN," in *Proc. IEEE Int. Rel. Phys. Symp. (IRPS)*, Apr. 2017, pp. XT-9.1–XT-9.5, doi: 10.1109/IRPS.2017.7936423.

[20] F. M. Puglisi and P. Pavan, "RTN analysis with FHMM as a tool for multi-trap characterization in HfOX RRAM," in *Proc. IEEE Int. Conf. Electron Devices Solid-state Circuits*, Jun. 2013, pp. 1–2, doi: 10.1109/EDSSC.2013.6628059.

[21] K. Abe, A. Teramoto, S. Sugawa, and T. Ohmi, "Understanding of traps causing random telegraph noise based on experimentally extracted time constants and amplitude," in *Proc. Int. Rel. Phys. Symp.*, Apr. 2011, doi: 10.1109/IRPS.2011.5784503.